Position Estimation and Error Analysis in Linear Switched Reluctance Motors

Shi Wei Zhao, *Member, IEEE*, Norbert C. Cheung, *Senior Member, IEEE*, Wai-Chuen Gan, *Senior Member, IEEE*, and Jin Ming Yang

***Abstract*—In this paper, a continuous position estimation scheme is presented for linear switched reluctance motors (LSRMs). The scheme uses diagnostic current injection into an unenergized phase to detect the motor position. This paper proposed that a new current integration index be used to quantify the measurement of current waveform. Hardware implementation results demonstrate the effectiveness of the proposed estimation scheme for the LSRM. This paper also performs a study on the accuracy of the estimated position. Through the detailed experimental data, the approach of polynomial fitting is compared with the lookup table with regard to characteristic curve representation. The estimation error distributions and their standard deviation show that the accuracy and precision are close between these two approaches.**

***Index Terms*—Error analysis, linear switched reluctance motor (LSRM), position estimation.**

I. Introduction

LINEAR switched reluctance motors (LSRMs) have received considerable attention for industrial applications in recent years. Compared with rotary motors with transformation components for linear motion, LSRMs have many advantages, e.g., quick response, high sensitivity, and position tracking capability. The structure of LSRMs can reduce the space requirement for their installation. Moreover, LSRMs have a simpler more rugged structure and a lower system cost than that of a direct drive permanent magnet linear synchronous motor. These reasons make LSRMs an alternative choice for direct-drive applications. However, the requirement for a direct position sensor to synchronously commutate the current from phase to phase and feedback the position information has excluded the motor from many cost-sensitive applications.

In the last two decades, several indirect position estimation schemes have been proposed for rotary switched reluctance motors (RSRMs). Some of the schemes use the phase inductance variation to detect the rotor position [1]–[6], whereas others obtain the position information from their phase flux linkage [7]–[9]. These schemes stem from the fact that both of the phase inductance and the phase flux linkage are functions of the rotor position and the phase current. The basic principle of incremental inductance was originally proposed in [1]. By investigating the waveforms of phase current, this method mainly considers the relationship between incremental inductance and position. In [2]–[4], the incremental inductance was estimated by injecting a diagnostic current to an unenergized phase and respectively measuring the current with respect to Δi, frequency, and phase. In [5], an estimation scheme based on incremental inductance was proposed by using hardware circuit to detect the current rise of the pulse-width modulated (PWM) waveform. One analytical model of incremental inductance in terms of Fourier series was reported in [6]. In [7], a nonintrusive rotor position estimation was proposed, which relies on the machine's inherent flux/current magnetic characteristics to infer the rotor position from measurements of stator flux linkage and current during normal phase excitation. Considering the eddy current effects, a correction factor was introduced in [8], and a principle of high-resolution position estimation was proposed in [9], which uses either flux linkage or current to correct errors in the rotor position through the correlation of current, flux linkage, and rotor position. In [10], an analytical prediction by using Fourier series for the inductance profile of an LSRM was developed. One method of flux-linkage measurement by using the digital integration of the induced electromotive force (EMF) from a search coil was proposed in [11]. By directly using the winding voltage, another digital integration method was reported [12]. The effects of cross magnetization and saturation on the inductances of a linear synchronous reluctance motor were discussed in [13]. Then, an experimental approach for the identification of linear synchronous reluctance motor parameters was proposed in [14].

In spite of the numerous publications in RSRMs, there are few literatures that refer to the position estimation of LSRMs. Compared with RSRMs, LSRMs have three disadvantages with regard to position estimation. First, many schemes use the inductance variation information to extract their position, because the phase inductance of an RSRM significantly varies. The ratio of the maximum to the minimum inductance in RSRMs is usually three or even greater, whereas the inductance of the proposed LSRM is only about 1.25, and an LSRM usually has a larger air gap. For LSRMs, the attraction force directly acts downward on their moving platform, whereas in the case of RSRMs, the attraction force can be balanced by the stator pole and its diametrically opposite pole when excited. This

Manuscript received August 7, 2007; revised March 28, 2008. This work was supported in part by the University Grants Council through Project Code PolyU 5224/04E and the South China University of Technology through the National Natural Science Foundation of China under Grant 60674099. The review of this paper was coordinated by Associate Editor Dr. Jerome Blair.

S. W. Zhao and N. C. Cheung are with the Department of Electrical Engineering, Hong Kong Polytechnic University, Kowloon, Hong Kong (e-mail: eencheun@ inet.polyu.edu.hk).

W.-C. Gan is with ASM Assembly Automation, Ltd., Kwai Chung, Hong Kong.

J. M. Yang is with the Electric Power College, South China University of Technology, Guangzhou 510640, China.

Digital Object Identifier 10.1109/TIM.2009.2016363

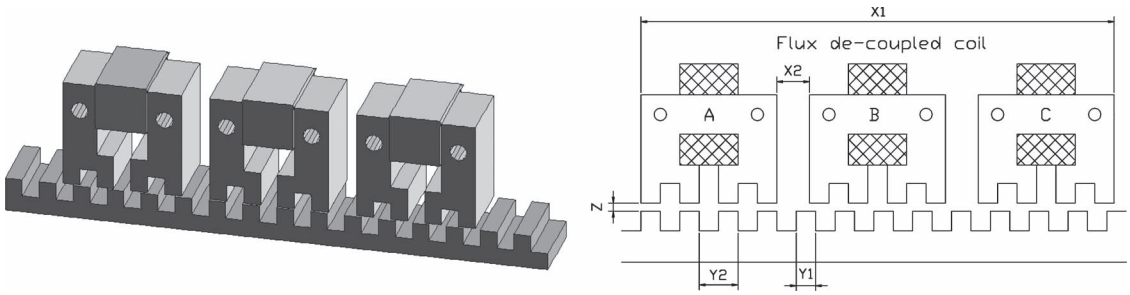

Fig. 1. Schematic of the LSRM.

instance indicates that the sensitivity of inductance to position for an LSRM is much lower than that of an RSRM, and the estimation accuracy is prone to measurement noise. Second, many RSRMs operate under the speed control, whereas LSRMs are usually applied in position control and trajectory control [15] and [16]. The position estimation for RSRMs, therefore, is usually to require some special discrete position signals for their commutation and speed estimation, whereas for LSRMs, the estimated position information is required to be more detailed for the commutation, real-time position feedback, and current calculations. Last, under the speed control mode, phase current and flux linkage for RSRMs periodically vary, whereas those for LSRMs are not very periodical and more complicated due to position or trajectory control.

This paper provides a continuous position estimation scheme for LSRMs. By injecting a series of periodically diagnostic current into an unenergized phase, the position is extracted from the measurement of the current. For LSRMs, the main advantages of this position estimation scheme can be summarized as follows.

1) This scheme requires no additional hardware for implementation, and the diagnostic current is generated by its main converter.
2) It requires no massive experimental data to calculate the magnetization curves, because the position is estimated using a simple characteristic curve.
3) The estimation scheme has no relationship with load.
4) At low speed, the estimation precision is insensitive to velocity variation, although this scheme is not applicable for very high speed.

Due to the travel distance limitation, LSRM's operation is usually restricted to only medium- or low-speed operation. Hence, this position estimation scheme is suitable for the LSRM.

According to the diagnostic current, current rise and current integration are used to quantify the measurement of current waveform. With the two indexes, a one-to-one relationship is built up between the motor position and the diagnostic current. In turn, the motor position is estimated using the relationship. In addition, two approaches—polynomial fitting and lookup table—are compared to represent the characteristic curve.

II. Proposed Method

A. Construction and Model of the LSRM

The proposed LSRM is a three-phase motor, and its design schematic is shown in Fig. 1. This LSRM comprises two components: 1) the moving platform and 2) the stator track. A set of three-phase coils with the same dimensions is installed on the moving platform. The three-phase windings are separated 120 electrical degrees from each other. The body of the moving platform is manufactured with aluminum so that the total weight of the moving platform and its inertia are low and the magnetic paths are decoupled. The moving platform is mounted on two slider blocks that are tightly fixed on the bottom of the LSRM. The linear guides are located between the moving platform and the slider blocks. This rugged mechanical structure can effectively buffer extended vibration during its operation. In addition, the stator track is fixed on the base of the LSRM. The stator track and the core of the windings are laminated with 0.5-mm silicon-steel plates, through which the motor manufacture can be simplified, and the total cost is greatly reduced.

For the LSRM, any one of the three phases on the moving platform is referred to be aligned, where its teeth fully correspond to any teeth on the stator track. In this position, the phase reluctance has a minimum value. A phase position is referred to be unaligned, where the teeth of the phase fully correspond to the slots of the stator track, and the phase reluctance achieves its maximum value there.

For a three-phase LSRM, the fundamental equation of each phase winding is given by the following voltage balancing equation (1), where j is the phase index, v_j is the phase voltage applied to the terminals, i_j is the phase current, r_j is the resistance of the coil, and λ_j is the phase flux linkage:

$$v_j = r_j i_j + \frac{d\lambda_j}{dt}, \qquad j = a, b, c. \tag{1}$$

Both the flux linkage λ_j and the phase inductance L_j are functions of the phase current i_j and the displacement x of the moving platform; thus, (1) can be expanded as (2) and (3). The fourth term in the right-hand side of (3) is defined as the motional EMF, which would be significant in high speed but can be negligible in low speed. We have

$$v_j = r_j i_j + \frac{\partial \lambda_j}{\partial i_j}\frac{di_j}{dt} + \frac{\partial \lambda_j}{\partial x}\frac{dx}{dt}, \quad j = a, b, c \tag{2}$$

$$v_j = r_j i_j + L_j \frac{di_j}{dt} + i_j \frac{\partial L_j}{\partial i_j}\frac{di_j}{dt} + \frac{\partial \lambda_j}{\partial x}\frac{dx}{dt}, \quad j = a, b, c. \tag{3}$$

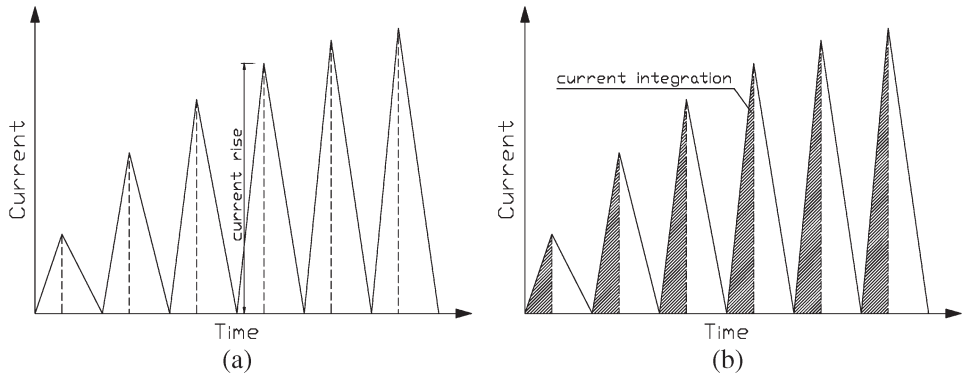

Fig. 2. Measuring (a) the current rise and (b) the current integration from a diagnostic-phase current waveform.

B. Position Information From the Phase Current

As the description in voltage balancing equation (1)–(3), the position information is stored in the phase inductance and phase flux linkage. It is shown that the position is difficult to extract by accurately solving the equations due to their complexities. The voltage balancing equation, however, can be approximated by some simple forms in special cases. In these situations, the position can simply be represented by the phase current, and the position can then be obtained from measurements of the phase current. Two schemes for position detection have been proposed to measure Δi of an unenergized phase and di/dt in an energized winding in [2] and [5], respectively.

Assuming that the terminal voltage applies to a phase winding for an interval that is short enough to enable phase inductance to remain constant, the phase current can then be represented as a function of its phase inductance. Position information can be derived using its phase current waveform, because phase inductance corresponds to position. In this case, the phase current remains small, and the flux linkage of phase winding is in the linear region. The third term in the right hand of (3) can be treated zero, because phase inductance only varies with its position in a linear region. Moreover, the motional EMF, which is proportional to its speed, is insignificant. Therefore, it can also be ignored when the motor speed is not very high. This situation is consistent with actual operations of LSRMs, because the short travel distances limit their maximum speeds. Hence, (3) can be approximated as (4) by neglecting the third and fourth terms in its right hand, i.e.,

$$v_j = r_j i_j + L_j \frac{di_j}{dt}, \qquad j = a, b, c. \tag{4}$$

By solving (4) for phase inductance, position information can directly be extracted from phase inductance or measurements of di/dt. In general, the computation time for obtaining phase inductance in real time would result in the requirement of powerful processors. Hence, the scheme by measuring di/dt is more popular for its simple implementation. Another approach is to solve the equation for its current as

$$i_j(t) = \frac{B_j}{A_j} v_j (1 - e^{-A_j t}), \qquad j = a, b, c \tag{5}$$

where $A_j = r_j/L_j$, $B_j = 1/L_j$, and the initial phase current is zero. It is clear that the phase current profile depends on the phase inductance for a constant phase resistance and a given duration. The position, therefore, can directly be extracted from the phase current profile, because inductance corresponds to position.

It is obvious that the phase current profile is difficult to directly be used in position calculation. However, it can be applied in position estimation after quantification. For a given interval Δt, a phase current profile of phase j can be quantified by its current rise, which can be calculated from (6). In addition, a phase current waveform can be quantified by the current integration I_j as (7). Current rise or current integration is a quantitative index for describing the characteristics of the phase current profile. A one-to-one relationship between position and current rise or current integration can be built up by recording the index value for each position. Moreover, position can be obtained by matching the actual index with the index from the one-to-one relationship. We have

$$i_j(t) = \frac{B_j}{A_j} v_j (1 - e^{-A_j \Delta t}), \qquad j = a, b, c \tag{6}$$

$$I_j = \int_0^{\Delta t} i_j(\tau) d\tau, \qquad j = a, b, c. \tag{7}$$

The concept of the current rise and current integration for position estimation is shown in Fig. 2. The phase current profile in each period corresponds to a certain position where the inductance is different. It is clear that both the rise on the current waveform and the area enclosed by the current waveform would vary with different current waveforms for a given interval. The measurement of the current rise aims at obtaining the difference between the first sample point and the last sample point of the current during the increase region for each period, and the measurement of current integration aims at calculating the sum of each sample point during its increase region. For each period, the triangle current waveforms can be indexed by their height according to the current rise or by their area according to the current integration. Hence, both the current rise and the current integration are a kind of quantitative description of the phase current waveform for each measurement period.

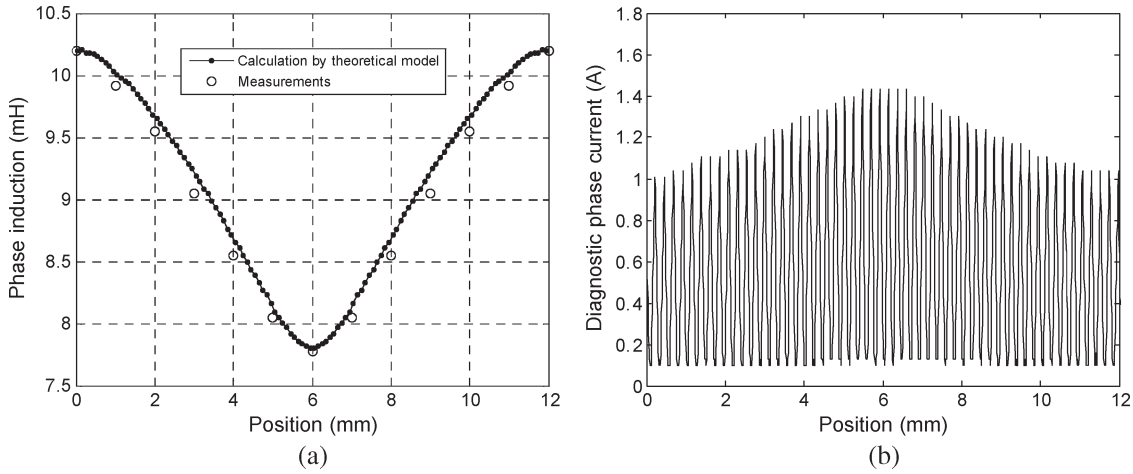

Fig. 3. Profile of (a) the phase inductance and (b) the waveform of the diagnostic-phase current versus the pole pitch length.

C. Position Estimation of the LSRM

For a three-phase LSRM, there is, at least, one phase that needs to be unenergized for multiphase excitation, and there are two phases that need to be unenergized for single-phase excitation during its operation. This step provides the possibility of using these unenergized phases for position estimation. To satisfy the aforementioned imposed assumptions for position estimation, one feasible scheme is to periodically inject a series of very small current pulses into an unenergized phase. In each period, the phase current is first built up by applying terminal voltage to phase windings, and then, the phase current is discharged to zero by inversely connecting a voltage source with it. For the selection of period, the interval should be short enough to guarantee that the value of the phase inductance is invariable for each period. On the other hand, the duty ratio of the periods should slightly be smaller than 0.5 to fully discharge the phase current to zero in each period to achieve the same initial condition for each measurement period.

The position estimation of the LSRM can be divided into two steps. The first step is to find a quantitative index to describe the diagnostic current waveform for each measurement period, e.g., current rise or current integration. Based on the index, the characteristic relationship between the position and the current can be built up. The second step is to find a suitable format to represent the characteristic relationship for position estimation, e.g., lookup table or polynomial fitting.

A lookup table is a common method for describing nonlinear relationships, because it can be implemented in some low-power processors. To form a lookup table, experimental data of the current rise or the current integration is first divided into different groups of the selected dimension according to position. For each group, the average of its experimental data is regarded as the characteristic point. The characteristic relationship is then represented by considering all the characteristic points. However, building up a lookup table, particularly a high-precision lookup table, from lots of experimental data would spend a long time. Compared to the approach of lookup table, fitting a nonlinear relationship by using polynomials is much easier. The characteristic relationship is represented as the coefficients of a polynomial that best fit the experimental data in a least square sense. With the industrial development, more high-speed processors are available, which provide the basis of polynomial fitting.

Fig. 3 shows the profile of a phase inductance and the diagnostic phase current in a pole pitch for the proposed LSRM. In this figure, the inductance profile of the theoretical model denotes the calculation results by using (4) and the diagnostic phase current. In addition, the points marked by circles denote the measured values in different positions by the inductance meter. The motional EMF in (3) is neglected in the inductance calculation model (4), and the measured values are a bit different from those of theoretical calculation. However, it can be observed that the theoretical results are in good agreement with the measured values. In these figures, 0 mm corresponds to the fully aligned position, and 6 mm corresponds to the fully unaligned position. It is clear that the diagnostic phase current reaches its maximum point at the unaligned position, where the minimum phase inductance achieves. On the other hand, the diagnostic phase current reaches the minimum current at the aligned position, where the maximum phase inductance achieves. Notice that the relationships between the phase inductance, the diagnostic phase current, and the position are monotonic only in a pole width. Hence, the position estimated within the range of a pole width can uniquely be obtained from the measurement and calculation of the diagnostic current. The position estimation for a pole pitch requires knowing that the current position is ranged the half from 0 to 6 mm or in another half. This problem can be solved by the injection of diagnostic current into two phases, because when one phase is near the terminal region, the other phase must be in its midway. This condition is shown in Fig. 1. The three-phase windings are separated 120 electrical degrees from each other. As a result, the precision of the position estimation for full range eventually depends on the estimation precision in each pole width.

D. Error Analysis of Position Estimation

In this section, error analysis of position estimation is investigated from the measurement error of the phase current, terminal

voltage ripples, and speed variation, because these three factors are directly related to the phase current.

For the estimation approach by using current rise, the measurement error of the phase current denotes the measurement error for the maximum current in each current period. According to (6), current error Δi_j from terminal voltage ripples Δv_j can be represented as (8). For simplicity, the motional EMF can usually be described as (9), and the current error from speed variation can be written as (10), i.e.,

$$\Delta i_j(t) = k_j \Delta v_j, \quad k_j = \frac{1 - e^{-A_j \Delta t}}{r_j}, \quad j = a, b, c \tag{8}$$

$$\frac{\partial \lambda_j}{\partial x}\frac{dx}{dt} = k'_j \frac{dx}{dt}, \quad j = a, b, c \tag{9}$$

$$\Delta i_j(t) = k_j k'_j \frac{dx}{dt}, \quad j = a, b, c. \tag{10}$$

For the estimation approach by using current integration, the current integration error from the measurement error of the phase current can be represented as (11). According to (8), current integration error ΔI_j from terminal voltage ripples Δv_j can be approximated as (12), and the current integration error from speed variation can be written as (13), i.e.,

$$\Delta I_j = \int_0^{\Delta t} \Delta i_j(\tau) d\tau, \qquad j = a, b, c \tag{11}$$

$$\Delta I_j = \int_0^{\Delta t} k_j \Delta v_j(\tau) d\tau, \qquad j = a, b, c \tag{12}$$

$$\Delta I_j = \int_0^{\Delta t} k_j k'_j \frac{dx}{dt}(\tau) d\tau, \qquad j = a, b, c. \tag{13}$$

Assuming that the position in a pole width y_1 is represented as $x = f_j(i_j)$ by the current rise, a current rise error of Δi_j yields a corresponding position estimation error as

$$|\Delta x| = \left| \frac{df_j}{di_j} \Delta i_j \right|. \tag{14}$$

In addition, the position estimation error by a current integration error ΔI_j can be represented by (15) when the relationship between the position in a pole width and the current integration satisfies $x = F_j(I_j)$, i.e.,

$$|\Delta x| = \left| \frac{dF_j}{dI_j} \Delta I_j \right|. \tag{15}$$

The aforementioned analysis demonstrates that the measurement error of phase current, the terminal voltage ripples, and speed variation contribute to the position estimation error. As shown in (10) and (13), both the current rise error and the current integration error would be increased with speed. It further indicates that the estimation scheme is suited for low-speed operations of LSRMs, and it would lose its efficiency in high speed.

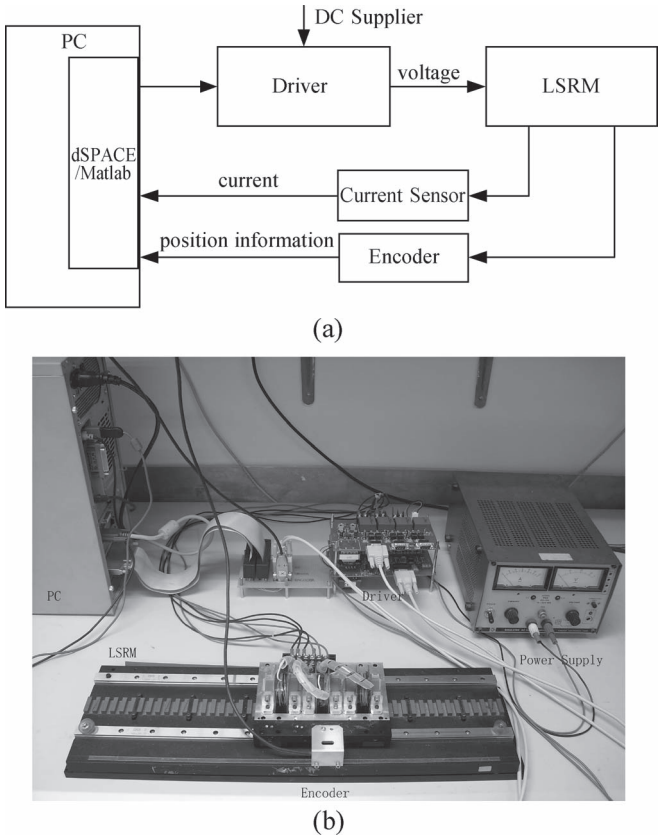

Fig. 4. Experimental setup. (a) The block diagram. (b) The overall appearance.

For simplicity, the position estimation error can be approximated by (16) and (17) when the position in a pole width is a linear function of the current rise or the current integration, i.e.,

$$|\Delta x| = y_1 \left| \frac{\Delta i_j}{i_{j\max} - i_{j\min}} \right| \tag{16}$$

$$|\Delta x| = y_1 \left| \frac{\Delta I_j}{I_{j\max} - I_{j\min}} \right| \tag{17}$$

where $i_{j\max}$ and $i_{j\min}$ indicate the current rise in an unaligned and aligned position, and $I_{j\max}$ and $I_{j\min}$ indicate the corresponding current integration. The two equations reveal that the position estimation error would benefit from a larger value of $i_{j\max} - i_{j\min}$ or $I_{j\max} - I_{j\min}$. It also implies that the estimation error can be reduced by increasing the ratio of the maximum to the minimum phase inductance and the terminal voltage according to (5).

III. Hardware Implementation

The experimental setup is shown in Fig. 4. The host PC is a Pentium 4 computer that is used to develop the estimation algorithm under the environment of MATLAB/SIMULINK and download the target code into a dSPACE DS1104 digital signal processing motion controller card, which is plugged into a peripheral component interconnect bus of the host PC. The PWM signals that the dSPACE card generated are sent to

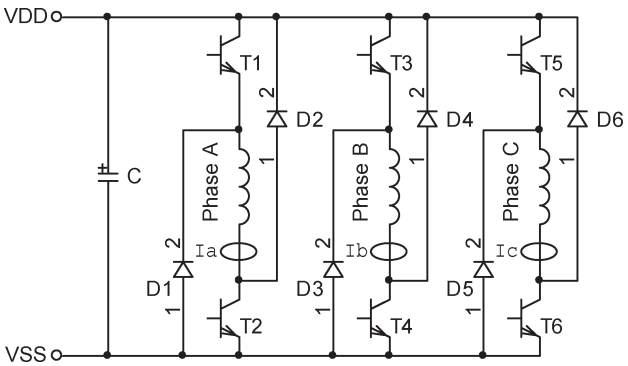

Fig. 5. Main converter circuit for a three-phase LSRM.

the main converter to drive the motor and produce diagnostic currents. The current values are obtained by the current sensors and sampled by the dSPACE card, in turn, to obtain the position information. A linear optical encoder with a 0.5-μm resolution is mounted on the mover of the LSRM system and provides position information for verification.

The drive circuit diagram for the three-phase LSRM is shown in Fig. 5. According to the main converter circuit, there are at most three operations for this converter circuit. For the first operation, the terminal voltage would be connected with the phase winding when both of the switches are closed in the phase and the phase current would be set up. For the second operation, the terminal voltage would reversely be connected with the corresponding phase winding by a pair of diodes, whereas the two switches in this phase are open, and the phase current is quickly discharged to the capacitor at the terminal. For the third operation, if only one switch is closed for one phase, the current in this phase would form a closed loop by the switch and a diode.

In actual operations, the converter requires generating high-level driving currents to drive the LSRM and low-level diagnostic currents to obtain position information. Correspondingly, the drive circuit has two operation modes: 1) the driving mode and 2) the sensing mode. During the driving mode, the bottom switch is always closed, whereas the top switch is operated with its duty cycle. Then, the current ripple can effectively be flatted. During the sensing mode, both switches of the phase are simultaneously operated with the same actions to generate high ripple and low-level diagnostic currents through the phase windings. In the experiments, the power supply is a 30-VDC voltage source. To obtain high estimation precision, the frequency of the diagnostic PWM signals is set to 1 kHz, and its duty ratio is 0.4.

IV. Analysis of the Experimental Data

Using the diagnostic current data in different positions, their relationship can be represented as a characteristic curve based on the index of the current waveform. Fig. 6 shows the results of the measured current data and their characteristic curves for the schemes of the current rise and the current integration, respectively. It is shown that both of the characteristic curves can well match their actual measured data. In addition, the measured data for the current-rise-based scheme are tightly distributed around its characteristic curve, as shown in Fig. 6(a). The measured data from the current-integration-based method have loose distributions according to its characteristic curve, as shown in Fig. 6(b). It infers that the current-rise-based scheme would have better estimation precision.

Fig. 7 shows the error distribution and the standard deviation of the position estimation for the two schemes. The bottom graph in Fig. 7(a) is the error distribution by using the current-rise-based scheme, whereas the top graph is the result for the current-integration-based scheme. Fig. 7(b) shows their standard deviation curves. It is clear that both of the schemes can effectively estimate the position, but the results from the current-rise-based estimation have better precision than those from the current-integration-based scheme for this system.

Fig. 8 shows the error distribution and the standard deviation of the position estimation by using polynomial fitting and lookup table to represent the characteristic curve. It is shown that accuracy and precision are close for the two approaches. In addition, notice that the estimation error displays different characteristics for different position regions, because the error that ranged $2-5$ mm has lower deviation than the error in the other regions for the proposed LSRM. The reason is that the characteristic curve has lower measurement sensitivity in the optimal region than that in other regions, as shown in Fig. 6. According to the experimental result, therefore, the position estimation can be expected to achieve higher precision in the optimal region.

Fig. 9 shows the results of position estimation by using the scheme of polynomial fitting based on the current rise. It is shown that the estimations for both relative position and absolute position are close to their actual positions. In addition, it is shown that the estimation error at the beginning stage is big, whereas the precision is improved in the later stage. The reason is that the high velocity in the beginning stage would generate an obvious motional EMF, which gradually decreases at the following stage when the motor slows down. For this experimental data, the average estimation error is 0.1 mm, and the standard deviation for the estimation is 0.17 mm. The experimental results demonstrate that the position estimation approach is effective and accurate for the LSRM.

V. Conclusion

In this paper, a continuous position estimation scheme for LSRMs is presented. The scheme uses diagnostic current pulses that were injected into an unenergized phase to detect the motor position. According to the diagnostic current, current rise and current integration are applied to quantify the measurement of current waveform and estimate the LSRM position. This paper has also conducted a detailed error analysis to investigate the position estimation accuracy from the measurement error of the phase current, terminal voltage ripples, and speed change. This analysis further confirmed that the proposed estimation scheme is suitable for LSRMs.

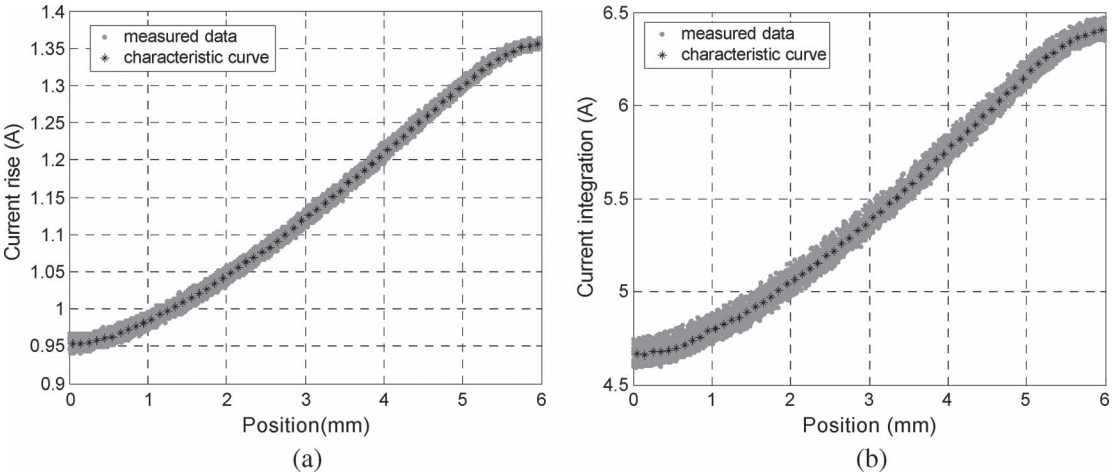

Fig. 6. Measured data and their corresponding fitted characteristic curves. (a) Results by using the scheme of current rise. (b) Results by using the scheme of current integration.

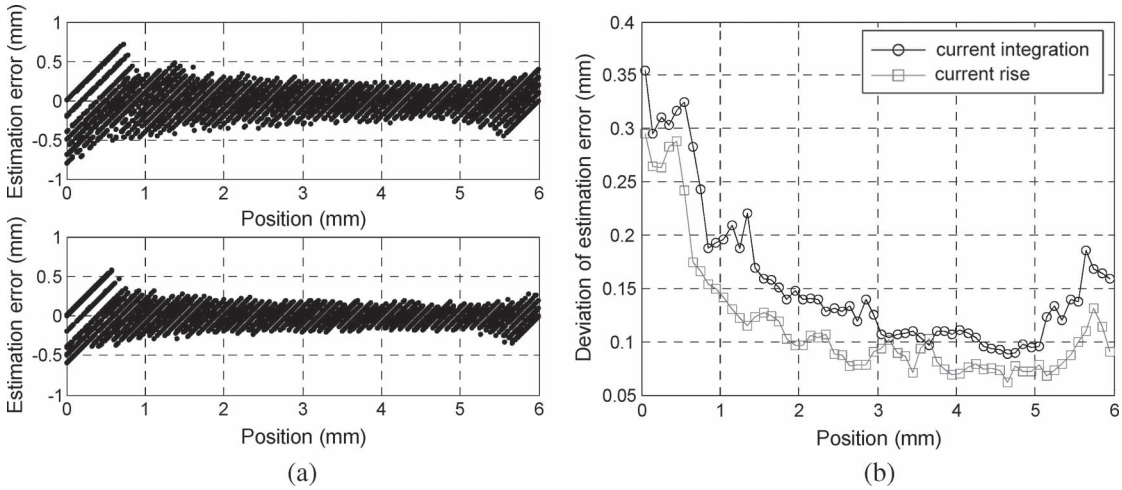

Fig. 7. Error distribution and standard deviation versus position in a pole width. (a) Error distribution by using (top) the current integration and (bottom) the current rise. (b) Standard deviation versus position in a pole width.

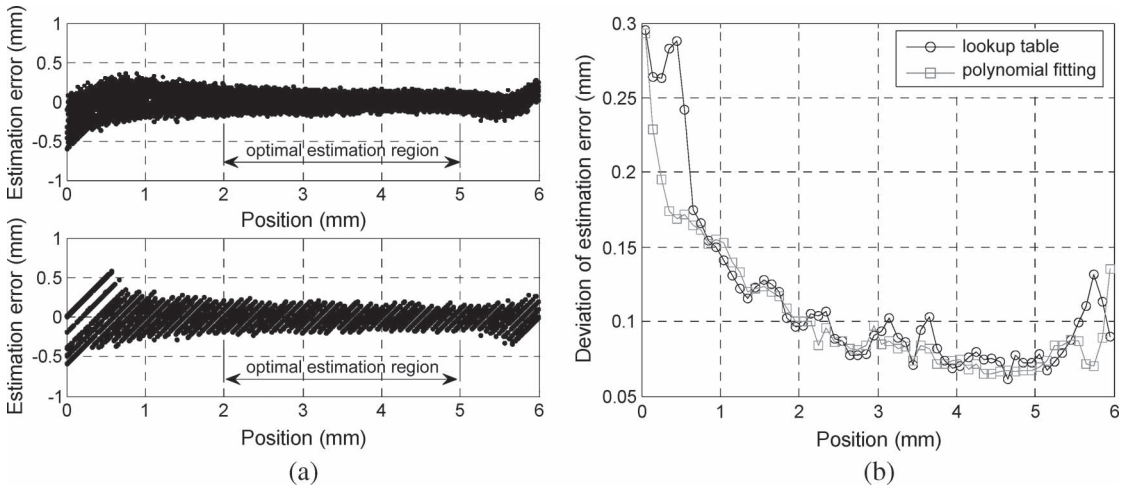

Fig. 8. Error distribution and standard deviation versus position in a pole width. (a) Error distribution by using (top) polynomial fitting and (bottom) lookup table. (b) Standard deviation versus position in a pole width.

Hardware implementation results illustrate that the estimated position trajectory is close to its actual position profile. The detailed experimental data and error analysis demonstrate the effectiveness of using the current integration to represent the characteristic curve between the position and the measurement current. It also demonstrates that the position estimation

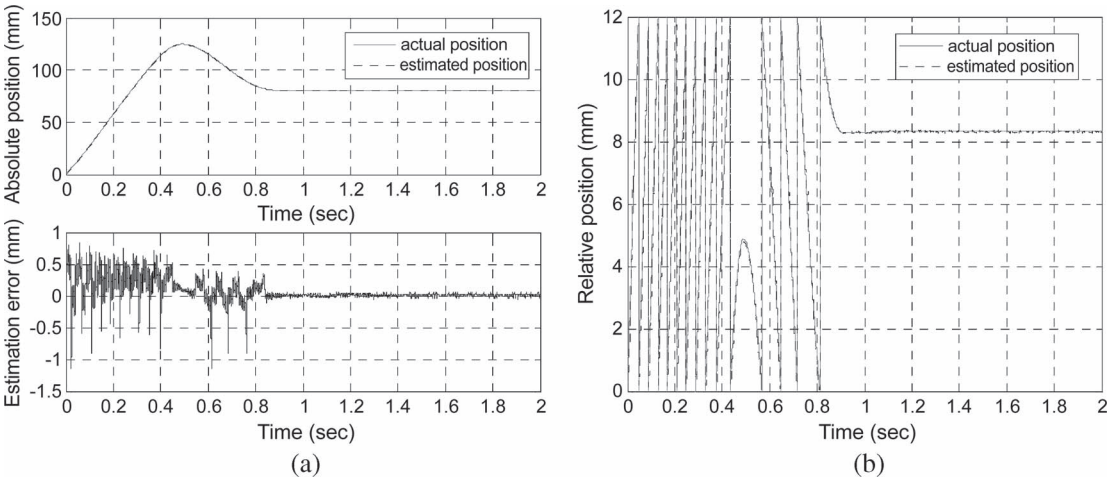

Fig. 9. Estimation result with probe phase selection. (a) Actual absolute position and its estimation, as shown at the top figure, and the error profile, as shown at the bottom figure. (b) Actual relative position and its estimation.

precision of this scheme is slightly inferior to the current-rise-based scheme. This paper has also compared the polynomial fitting with the lookup table in the characteristic curve representation. The estimation error distribution and the standard deviation show that the accuracy and precision are close for the two approaches. The experimental data also indicate one optimal estimation region due to high measurement sensitivity in this region.

APPENDIX

TABLE I
ELECTRICAL AND MECHANICAL PARAMETERS OF THE LSRM

Max travel distance	300mm
Motor length (x_1)	146mm
Phase separation (x_2)	10mm
Pole width (y_1)	6mm
Pole pitch (y_2)	12mm
Wind length	18mm
Wind width	25mm
Air gap width (z)	0.5mm
Phase resistance	1.5Ω
Aligned inductance	10.2mH
Unaligned inductance	7.8mH
Mass of the moving platform	1.8kg

ACKNOWLEDGMENT

The authors would like to thank Dr. X. D. Xue of Hong Kong Polytechnic University and the anonymous reviewers for their useful comments and suggestions.

REFERENCES

[1] P. P. Acarnley, R. J. Hill, and C. W. Hooper, "Detection of rotor position in stepping and switched motors by monitoring of current waveforms," *IEEE Trans. Ind. Electron.*, vol. IE-32, no. 3, pp. 215–222, Aug. 1985.
[2] S. R. MacMinn, W. J. Rzesos, P. M. Szczesny, and T. M. Jahns, "Application of sensor integration techniques to switched reluctance motor drives," in *Conf. Rec. IEEE-IAS Annu. Meeting*, Oct. 1988, pp. 584–588.
[3] M. Ehsani, I. Husain, and A. B. Kulkarni, "Elimination of discrete position sensor and current sensor in switched reluctance motor drives," *IEEE Trans. Ind. Appl.*, vol. 28, no. 1, pp. 128–135, Jan./Feb. 1992.
[4] M. Ehsani, I. Husain, S. Mahajan, and K. R. Ramani, "New modulation encoding techniques for indirect rotor position sensing in switched reluctance motors," *IEEE Trans. Ind. Appl.*, vol. 30, no. 1, pp. 85–91, Jan./Feb. 1994.
[5] M. F. Rahman, N. C. Cheung, and K. W. Lim, "Position estimation in solenoid actuators," *IEEE Trans. Ind. Appl.*, vol. 32, no. 3, pp. 552–559, May/Jun. 1996.
[6] H. Gao, F. R. Salmasi, and M. Ehsani, "Inductance model-based sensorless control of the switched reluctance motor drive at low speed," *IEEE Trans. Power Electron.*, vol. 19, no. 6, pp. 1568–1573, Nov. 2004.
[7] J. P. Lyons, S. R. MacMinn, and M. A. Preston, "Flux/current methods for SRM rotor position estimation," in *Conf. Rec. IEEE IAS Annu. Meeting*, 1991, pp. 482–487.
[8] D. Panda and V. Ramanarayanan, "An accurate position estimation method for switched reluctance motor drive," in *Proc. Int. Conf. Power Electron. Drives Energy Syst. Ind. Growth*, 1998, pp. 523–528.
[9] G. Gallegos-Lopez, P. C. Kjaer, and T. J. E. Miller, "High-grade position estimation for SRM drives using flux linkage/current correction model," *IEEE Trans. Ind. Appl.*, vol. 35, no. 4, pp. 859–869, Jul./Aug. 1999.
[10] S.-M. Jang, J.-H. Park, J.-Y. Choi, and H.-W. Cho, "Analytical prediction and measurements for inductance profile of linear switched reluctance motor," *IEEE Trans. Magn.*, vol. 42, no. 10, pp. 3428–3430, Oct. 2006.
[11] A. Ferro and A. Raciti, "A digital method for the determination of magnetic characteristics of variable reluctance motors," *IEEE Trans. Instrum. Meas.*, vol. 39, no. 4, pp. 604–608, Aug. 1990.
[12] A. D. Cheok and Z. Wang, "DSP-based automated error-reducing flux-linkage-measurement method for switched reluctance motors," *IEEE Trans. Instrum. Meas.*, vol. 56, no. 6, pp. 2245–2253, Dec. 2007.
[13] G. Stumberger, B. Stumberger, D. Dolinar, and A. Hamler, "Cross magnetization effect on inductances of linear synchronous reluctance motor under load conditions," *IEEE Trans. Magn.*, vol. 37, no. 5, pp. 3658–3662, Sep. 2001.
[14] G. Stumberger, B. Stumberger, and D. Dolinar, "Identification of linear synchronous reluctance motor parameters," *IEEE Trans. Ind. Appl.*, vol. 40, no. 5, pp. 1317–1324, Sep./Oct. 2004.
[15] W. C. Gan, N. C. Cheung, and L. Qiu, "Position control of linear switched reluctance motors for high-precision applications," *IEEE Trans. Ind. Appl.*, vol. 39, no. 5, pp. 1350–1362, Sep./Oct. 2003..
[16] S. W. Zhao, N. C. Cheung, W.-C. Gan, J. M. Yang, and J. F. Pan, "A self-tuning regulator for the high-precision position control of a linear switched reluctance motor," *IEEE Trans. Ind. Electron.*, vol. 54, no. 5, pp. 2425–2434, Oct. 2007.

Shi Wei Zhao (S'07–M'09) received the B.Sc. degree from Central South University, Changsha, China, in 2000, the M.Sc. degree from South China University of Technology, Guangzhou, China, in 2003, and the Ph.D. degree from Hong Kong Polytechnic University, Kowloon, Hong Kong, in 2008.

He is currently a Postdoctoral Fellow with the Department of Electrical Engineering, Hong Kong Polytechnic University. His main research interests are motion control, machine drives, and applications of renewable energy.

Norbert C. Cheung (S'85–M'91–SM'05) received the B.Sc. degree from the University of London, London, U.K., in 1981, the M.Sc. degree from the University of Hong Kong, Pokfulam, Hong Kong, in 1987, and the Ph.D. degree from the University of New South Wales, Kensington, U.K., in 1995.

He is currently with the Department of Electrical Engineering, Hong Kong Polytechnic University, Kowloon, Hong Kong. His research interests are motion control, actuators design, power electronic drives, measurement systems, and applications of renewable energy.

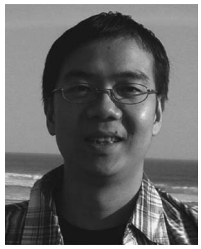

Wai-Chuen Gan (S'94–M'02–SM'06) received the B.Eng. degree (with First-Class Honors and the Academic Achievement Award) in electronic engineering and the M.Phil. and Ph.D. degrees in electrical and electronic engineering from Hong Kong University of Science and Technology, Clear Water Bay, Hong Kong, in 1995, 1997, and 2001, respectively.

From 1997 to 1999, he was a Motion Control Application Engineer with ASM Assembly Automation, Ltd., Kwai Chung, Hong Kong. He rejoined the same company in 2002 and is currently a Section Manager with the R&D Motion Group. His current research interests include robust control of ac machines, power electronics, design and control of linear switched reluctance motors, and linear permanent magnet motors.

Dr. Gan is a member of the Hong Kong Institution of Engineers.

Jin Ming Yang received the B.Sc. degree from the University of Beijing Aeronautics, Beijing, China, in 1987, the M.Sc. degree from Zhejiang University, Hangzhou, China, in 1990, and the Ph.D. degree from South China University of Technology, Guangzhou, China, in 2000.

He is currently an Associate Professor with South China University of Technology. His research interests are machine drives and nonlinear control.